Dressed photon-orbital states in a quantum dot: Intervalley spin resonance

P. Scarlino, E. Kawakami, T. Jullien, D. R. Ward, D. E. Savage, M. G. Lagally, Mark Friesen, S. N. Coppersmith, M. A. Eriksson, and L. M. K. Vandersypen

Phys. Rev. B **95**, 165429 — Published 19 April 2017

DOI: 10.1103/PhysRevB.95.165429

Dressed photon-orbital states in a quantum dot: Inter-valley spin resonance

P. Scarlino, E. Kawakami, and T. Jullien
Kavli Institute of Nanoscience, TU Delft, Lorentzweg 1, 2628 CJ Delft, The Netherlands

D. R. Ward, D. E. Savage, M. G. Lagally, Mark Friesen, S. N. Coppersmith, and M. A. Eriksson
University of Wisconsin-Madison, Madison, WI 53706, USA

L. M. K. Vandersypen
Kavli Institute of Nanoscience, TU Delft, Lorentzweg 1, 2628 CJ Delft, The Netherlands and
Components Research, Intel Corporation, 2501 NW 29th Ave, Hillsboro, OR 97124, USA
(Dated: February 27, 2017)

The valley degree of freedom is intrinsic to spin qubits in Si/SiGe quantum dots. It has been viewed alternately as a hazard, especially when the lowest valley-orbit splitting is small compared to the thermal energy, or as an asset, most prominently in proposals to use the valley degree of freedom itself as a qubit. Here we present experiments in which microwave electric field driving induces transitions between both valley-orbit and spin states. We show that this system is highly nonlinear and can be understood through the use of dressed photon-orbital states, enabling a unified understanding of the six microwave resonance lines we observe. Some of these resonances are inter-valley spin transitions that arise from a non-adiabatic process in which both the valley and the spin degree of freedom are excited simultaneously. For these transitions, involving a change in valley-orbit state, we find a tenfold increase in sensitivity to electric fields and electrical noise compared to pure spin transitions, strongly reducing the phase coherence when changes in valley-orbit index are incurred. In contrast to this non-adiabtaic transition, the pure spin transitions, whether arising from harmonic or subharmonic generation, are shown to be adiabatic in the orbital sector. The nonlinearity of the system is most strikingly manifest in the observation of a dynamical anti-crossing between a spin-flip, inter-valley transition and a three-photon transition enabled by the strong nonlinearity we find in this seemly simple system.

A spin-1/2 particle is the canonical two-level quantum system. Its energy level structure is extremely simple, consisting of just the spin-up and spin-down levels. Therefore, when performing spectroscopy on an elementary spin-1/2 particle such as an electron spin, only a single resonance is expected corresponding to the energy separation between the two levels.

Recent measurements have shown that the spectroscopic response of a single electron spin in a quantum dot can be much more complex than this simple picture suggests. This is particularly true when using electric-dipole spin resonance, where an oscillating electric field couples to the spin via spin-orbit coupling [1]. First, due to non-linearities in the response to oscillating driving fields, subharmonics can be observed [2–7], and the nonlinear response can even be exploited for driving coherent spin rotations [8]. Second, due to spin-orbit coupling, the exact electron spin resonance frequency in a given magnetic field depends on the orbital the electron occupies [9]. In silicon or germanium quantum dots, the conduction band valley is an additional degree of freedom [10–14], and the electron spin resonance frequency should depend on the valley state as well [14–19]. As a result, when valley or orbital energy splittings are comparable to or smaller than the thermal energy, thermal occupation of the respective levels leads to the observation of multiple closely spaced spin resonance frequencies [17].

The picture becomes even richer when considering transitions in which not only the spin state but also the orbital quantum number changes. Such phenomena are common in optically active dots [20], but have been observed also in electrostatically defined (double) quantum dots in the form of relaxation from spin triplet to spin singlet states [21, 22] and spin-flip photon-assisted tunneling [23, 24]. However, that work is all in semiconductor quantum dots with no valley degree of freedom, and the degree to which valleys -often treated as weakly coupled to each other and orbital states-couple to each other to enable microwave-driven transitions that change spin has not been explored. Furthermore, the investigation of resonant transitions involving the valley degree of freedom is very important in the context of the new qubit architecture recently proposed for Si quantum dots [25], based on the valley degree of freedom to encode and process quantum information.

Here, we report transitions where both the spin and valley-orbit state flip in a Si/SiGe quantum dot. We demonstrate that we can Stark shift the transitions, and we compare the sensitivity to electric fields to the case of pure spin transitions, including the impact on phase coherence. We find that the valley-orbit coupling strongly affects the coherence properties of the inter-valley spin resonances. We show that a theory incorporating a driven four-level system comprised of two valley-orbit and two spin states subject to strong ac driving provides

a consistent description of these transitions, as well as all the previously reported transitions for this system. This theory also explains the observation of a dynamical level repulsion, which can be understood effectively and compactly using a dressed-state formalism.

DEVICE AND SPECTROSCOPIC MEASUREMENTS

The device used for this experiment has been described in [17] (see Fig. S3). It is based on an undoped Si/SiGe heterostructure with two layers of electrostatic gates. Two accumulation gates are used to induce a two-dimensional electron gas (2DEG) in a 12 nm wide Si quantum well 37 nm below the surface and a set of depletion gates is used to form a single quantum dot in the 2DEG, and a charge sensor next to this dot. The dot is tuned so it is occupied by just one electron. Two micromagnets placed on top of the accumulation gates produce a local magnetic field gradient. The sample is attached to the mixing chamber of a dilution refrigerator with base temperature ∼25 mK and an electron temperature estimated from transport measurements of ∼150 mK. For the present gate voltage configuration, the valley splitting, E_{VS}, is comparable to the thermal energy, $k_B T_{el}$.

Microwave excitation applied to one of the gates oscillates the electron wave function back and forth in the dot, roughly along the x axis (Fig. S3). Because of the local magnetic field gradient $dB_\perp/dx$ ∼0.3 mT/nm [17], where $B_\perp$ is the component of the micromagnet field gradient perpendicular to the static magnetic field B_{ext}, the electron is then subject to an oscillating magnetic field [26, 27] and electron spin transitions can be induced when the excitation is resonant with the spin splitting. The spin-up probability $P_\uparrow$ in response to the microwave excitation is measured by repeated single-shot cycles (see section III.A of the Supplemental Material for details). The initialization and read-out procedures require a Zeeman splitting exceeding $k_B T_{el}$, which here restricts us to working at $B_{tot} > 450$ mT.

When varying the applied microwave frequency and external magnetic field, we observe six distinct resonance peaks [see Fig. 1(a)][28]. The two resonances labeled (1) and (2), not resolved on this scale, are two intra-valley spin resonances, one for each of the two lowest-lying valley states that are thermally occupied [17]. They exhibit a $T_2^* \sim 1$ μs and Rabi frequencies of order MHz. The two resonances labeled (3) and (4), similarly not resolved, arise from second harmonic driving of the two intra-valley spin flip transitions. These transitions too can be driven coherently, with Rabi frequencies comparable to those for the fundamental harmonic, as we reported in [8].

We focus here on the resonances labeled (5) and (6) in Fig. 1, which have not been discussed before. The frequency of resonance (5), $f_0^{(5)}$, is ∼7 GHz lower than the fundamental intra-valley spin resonance frequencies, $f_0^{(1)}$ and $f_0^{(2)}$. From the magnetic field dependence measured above 500 mT, we extract a g-factor of about 1.971 ± 0.002, close to but different from the g-factors for resonances (1) and (2) (1.99 [17]). The line width (Fig. 3(a) inset and Fig. S4) is almost ten times larger than that for the intra-valley resonances, giving a correspondingly shorter T_2^* of around 100 ns. Around 500 mT, resonance (5) changes in a way reminiscent of level repulsions and transitions into resonance (6) (see Fig. 1(b)). Without the change in slope, resonance (5) would have crossed resonances (3) and (4); however, the latter do not show any sign of level repulsion and continue their linear dependence on magnetic field.

We interpret these puzzling observations starting with Fig. 1(d). Two sets of Zeeman split levels are seen, separated by the energy of the first excited valley-orbit state. The green (1) [(2)] and two blue (3) [(4)] arrows show driving of spin transitions via the fundamental and second harmonic respectively, for the valley-orbit ground [excited] state. We identify resonance (5) with the transition indicated with the red arrow in which both spin and valley(-orbit) flip. It has the same field dependence as resonance (1), but (above 500 mT) it is offset from resonance (1) by a fixed amount, which as we can see from Fig. 1(d), is a measure of the valley-orbit splitting, E_{VS}. Resonance (6) is a three photon process in which both spin and valley-orbit states flip. As we discuss below, hybridization between (5) and (6) is possible at magnetic fields $B_{tot} = \frac{2E_{VS}}{g\mu_B}$, for which the photons shown by the corresponding arrows in Fig. 1(d) have the same energy.

MODEL

We now introduce a simple model Hamiltonian that can be used to understand the observed spectroscopic response. This model explains the presence of both the first and second harmonic driven spin resonance as well as the observed inter-valley spin resonance. We show that resonances such as those observed in Fig. 1(a,b) are generic features of a strongly driven four-level system composed of two orbital levels and two spin levels in which there is a coupling between the orbital levels, such as a tunnel coupling. For our case, it is natural to associate the orbital levels with two different valley-orbit states (see section I of the Supplemental Material for details).

Our analysis builds upon the theory proposed by Rashba [29]. When a spin qubit is driven at a frequency ω, it responds at one or more frequencies Ω, which may be the same as ω, but may also be different (see Fig. 2(a)). Spin resonance is observed if (i) the spin is flipped [30], and (ii) $\hbar\Omega = E_Z$, where $E_Z = g\mu_B B_{tot}$ is the Zeeman splitting, g is the Landé g-factor in silicon, μ_B is the Bohr

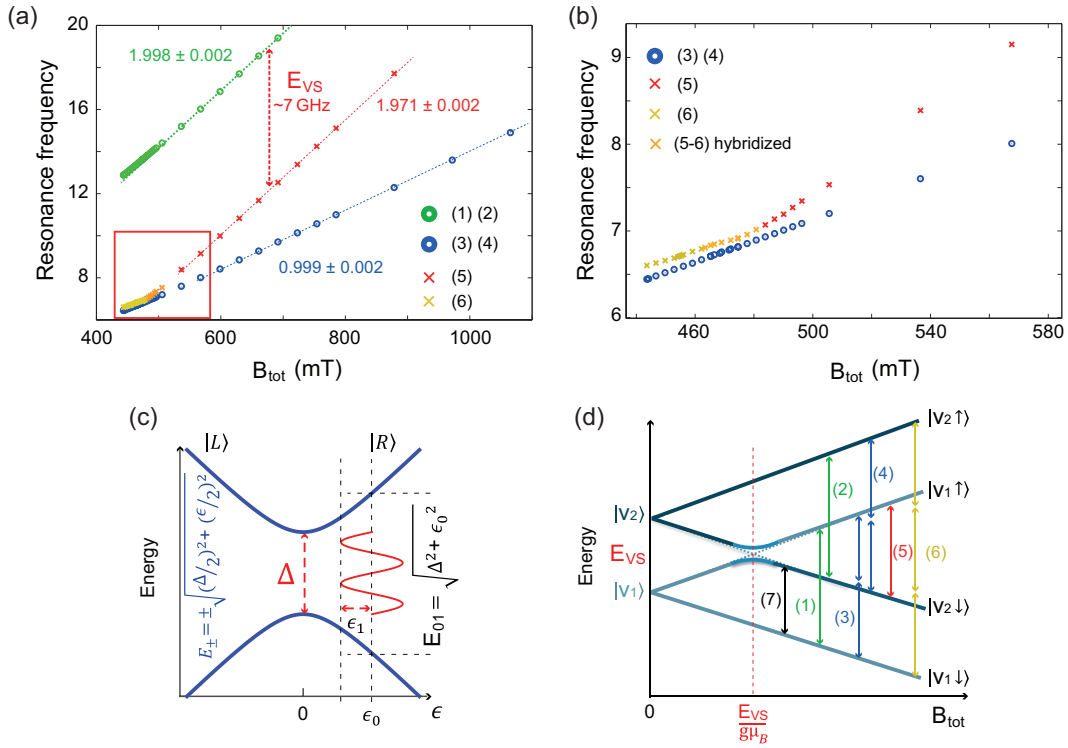

FIG. 1. (a) Multiple resonance frequencies as a function of the external magnetic field, observed for a single electron spin confined in a gate-defined Si/SiGe quantum dot, driven by low-power microwave excitation applied to one of the quantum dot gates. Resonances (1) and (2) are indistinguishable on this scale, as are resonances (3) and (4). On the horizontal axis, we plot $B_{tot} = \sqrt{(B^x_{ext} + B_\parallel)^2 + B^2_\perp}$, with $B_\parallel \sim -120$ mT and $B_\perp \sim 50$ mT the estimated components of the stray magnetic field from the micromagnet [magnetized, in this measurement, along the x-direction (see Fig. S3)]. (b) Zoom-in of the region indicated by a red box in panel (a). (c) Schematic energy level diagram of a generic two-level quantum system described by Eq. 1, as a function of detuning ϵ and with a harmonic driving of amplitude ϵ_1 around the central value ϵ_0 with energy eigenvalues $E_\pm$ and energy splitting $E_{01} = E_+ - E_-$. (d) The four energy levels considered in this work as a function of B_{tot}, in the absence of photonic dressing, comprised of two valley-orbit states ($|V_{1,2}\rangle$) and two spin states ($|\downarrow,\uparrow\rangle$). E_{VS} represents the valley-orbit energy splitting. The vertical arrows labelled 1-6 correspond to 6 processes observed in our simulations and to excitations observed in the experiment, with the same labeling scheme as panels (a) and (b). (1) and (2) correspond to single-photon spin flips. (3) and (4) correspond to two-photon spin flips. (5) corresponds to a combined spin flip, valley-orbit excitation, and single-photon absorption. (6) is also a combined spin-flip, valley-orbit excitation, between different states than (5), and is a three-photon process. (7) is a nonadiabatic valley-orbit excitation; it is observed in simulations but not in the experiments, because $E_{\rm VS} \sim k_B T_{\rm el}$, and therefore readout is ineffective.

magneton, and B_{tot} is the total magnetic field. In electric dipole spin resonance (EDSR), the spin flip requires a physical mechanism for the electric field to couple to the spin, such as spin-orbit coupling [26]. In our experiment, an effective spin-orbit coupling due to the strong magnetic field gradient from the micromagnet is the mechanism responsible for spin flips [17]. Hence, we can say that EDSR and its associated spin dynamics provide a tool for observing the mapping $\omega \to \Omega$. However, as discussed in [29], EDSR does not determine the mapping; determining the resonant frequencies Ω requires including the essential non-linearity in the system, which in this case resides in the orbital sector of the qubit Hamiltonian. We therefore focus on the dynamics of the orbital sector of the Hamiltonian; the mechanism for spin flips is included perturbatively after the charge dynamics have been characterized.

The exact orbital Hamiltonian is difficult to write down from first principles, since it likely involves both orbital and valley components [17], and depends on the atomistic details of the quantum well interface [10–12]. Nonetheless, the features of the resonances in Fig. 1 emerge quite naturally using a model with one low-lying orbital excited state. Referring to Fig. 1(c), in this model, the Hamiltonian for the orbital sector is described by a simple two-state Hamiltonian, which we write as

$$H = \frac{1}{2}(\epsilon\sigma_z + \Delta\sigma_x). \tag{1}$$

Here, ϵ is a detuning parameter, Δ is the tunnel coupling between the generic basis states labeled $|L\rangle$ and $|R\rangle$, and σ_x and σ_z are Pauli matrices. We consider a classical ac

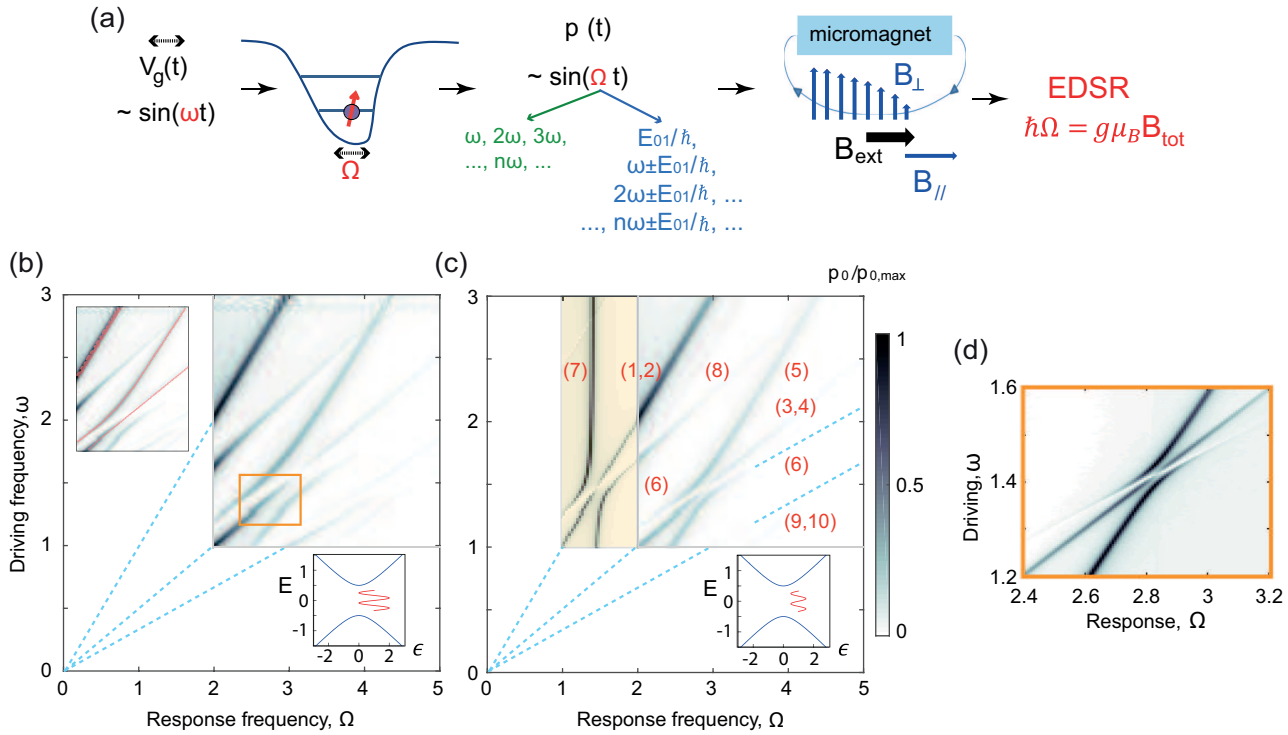

FIG. 2. Theoretical calculations of resonances in an ac-driven qubit with a low-lying orbital state induced by adiabatic and non-adiabatic processes. (a) Schematic illustrating that an excitation at driving frequency ω leads to several adiabatic (non-adiabatic) response frequencies of the electron dipole moment, $p(\Omega) = FFT[p(t)]$, listed in green (blue). The time-dependent electron dipole moment in turn produces spin flips due to the magnetic field gradient when $\hbar\Omega$ matches the Zeeman splitting. (b) Simulated resonance spectrum of the ac-driven qubit model of Eqs. (1) and (2), setting $\hbar = 1$. As described in the main text, the dynamics of the dipole moment $p(t)$, defined in Eq. (3), are solved in the time domain for the driving frequency ω, then Fourier transformed to obtain the response frequency Ω. Here we use $\epsilon_0 = \epsilon_1 = \Delta = 1$. The dashed lines indicate the positions of the fundamental resonance and its first two harmonics (top to bottom). The lower inset shows the relation between the energy levels and the driving term. The upper inset shows the same results as the main panel, with the experimentally relevant resonances highlighted (compare to Fig. 1). (c) Resonance spectrum corresponding to the parameters $\epsilon_0 = \Delta = 1$ and $\epsilon_1 = 0.5$. Here, the shaded region was normalized separately from the rest of the figure. The resonance features labeled 1-10 are discussed in the main text (see also sections I.C and II.B of Supplemental Material). (d) A blowup of the region shown in the center box of panel (b), using the parameters $\Delta = \epsilon_0 = 1$ and $\epsilon_1 = 0.11$, which gives good agreement with the level repulsion observed in the experiments shown in Figs. 1(a) and 1(b).

drive, applied to the detuning parameter:

$$\epsilon(t) = \epsilon_0 + \epsilon_1 \sin(\omega t). \tag{2}$$

If the quantum dot confinement were purely parabolic, then changing the detuning would not affect the energy splitting between the eigenstates. However, any non-parabolicity in the dot, which is unavoidable in real devices, will cause the energy splitting to depend on the detuning and will yield a nonlinear response to the driving term, Eq. 2. In our Hamiltonian, this effect enters via the tunnel coupling Δ, which causes the qubit frequency to depend on $\epsilon(t)$.

Our goal is to determine the response of the two-level system to this $\epsilon(t)$. We solve the time-dependent Schrödinger equation with the initial state $\psi(t = 0) = |0\rangle$ representing the adiabatic ground state of Eqs. (1) and (2) when $t = 0$, corresponding to $\epsilon_1 = 0$. We assume that the basis states are coupled by the applied electric field because they have different spatial charge distributions, and study the time evolution of the instantaneous dipole moment of the ground state $|0\rangle$, defined as

$$p(t) = \frac{eL}{2}\left[|\langle\psi(t)|L\rangle|^2 - |\langle\psi(t)|R\rangle|^2\right]. \tag{3}$$

Here, L is the distance between the charge in states $|L\rangle$ and $|R\rangle$ [31]

Rashba has studied Hamiltonian (1) perturbatively in the regime of weak driving and high excitation frequency [29]. In sections I and II of the Supplemental Material, we present a detailed exposition of our extensions of these investigations into the strong driving regime relevant to resonances (5) and (6). We find that driving this transition involves non-adiabatic processes [32–34] whereby the orbital state gets excited, in contrast to the subhar-

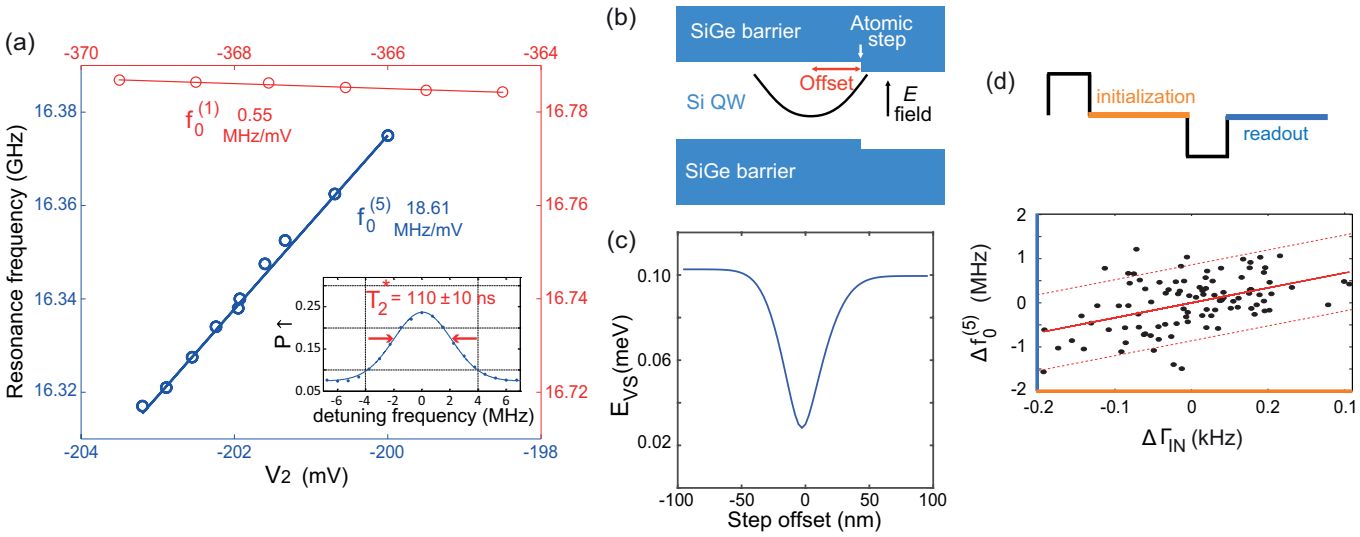

FIG. 3. Sensitivity of intra-valley and inter-valley spin transitions to electric fields. (a) Measured resonance frequency for the inter-valley ($f_0^{(5)}$ at B_{ext}^y =792 mT, blue data and axes) and intra-valley ($f_0^{(1)}$ at B_{ext}^y =550 mT, red data and axes) spin transition, as a function of gate voltage V_2. Inset: low-power continuous wave response of the inter-valley spin transition, with T_2^* estimated from the line width (see also Fig. S4). (b) Schematic representation of an atomic step in a Si/SiGe quantum well and of a quantum dot parabolic confinement potential (not to scale) laterally offset from the step. (c) Valley-orbit energy splitting found by a 2D tight binding calculation using the geometry shown in panel (b), a 13 nm wide quantum well barrier of 160 meV (corresponding to 30% Ge), a parabolic confinement potential for the dot of size $\sqrt{\langle x^2\rangle} = 21.1$ nm (corresponding to an orbital energy splitting of $\hbar\omega = 0.45$ meV), and an electric field of 1.5×10^6 V/m (the experimental electric field is not well known). In the plots, a positive step offset corresponds to a step on the right-hand side of the dot. (d) Scatter plot showing two quantities measured every 400 s. The x-axis shows the average rate, Γ_{IN}, with which an electron tunnels into the quantum dot during qubit initialization (in orange in the inset); on the y-axis is the frequency of resonance (5) relative to its value averaged over the entire measurement (see also Fig. S6). The continuous line represents a linear fit to the data through the point (0,0). The dashed lines represent the 95% confidence interval. The distribution of the points in the scatter plot indicates that the two quantities are correlated. $B_{ext}^x = 590$ mT, $B_{ext}^y = 598.2$ mT, $\Delta f_0^{(5)} = f_0^{(5)} - 15.6894$ GHz, $\Delta\Gamma_{IN} = \Gamma_{IN} - 1.0762$ kHz.

monics reported in [8], which as we show here involve only adiabatic processes in the charge sector.

Here, we present the results of numerical simulations in this regime and show that the results are consistent with the main features observed experimentally. The dynamical simulations are performed by setting $\hbar = 1$ and solving the Schrödinger equation $i\partial|\psi\rangle/\partial t = H|\psi\rangle$ for Eqs. (1) and (2) and computing $p(t)$ as defined in Eq. (3) for a fixed driving frequency ω [35]. The resulting $p(t)$ is Fourier transformed, yielding a $p(\Omega)$ whose peaks reflect the resonant response. Finally, we smooth $p(\Omega)$ by convolving it with a Gaussian of width 0.025 (in order to take into account noise, which is averaged in the experiment). Because of the spin-orbit coupling (the position-dependent transverse magnetic field from the micro magnet), spin and orbital states hybridize, and peaks in $p(\Omega)$ correspond to frequencies at which an ac magnetic field is generated that is resonant with the Zeeman frequency, $E_Z/\hbar = \Omega$, so spin flips will occur. The experiment measures the probability of a spin flip as a function of magnetic field; via the EDSR mechanism, resonances in this probability therefore occur when the peak locations in $p(\Omega)$ satisfy $g\mu_B B_{tot} = \hbar\Omega$.

Figs. 2(b) and (c) show the results of our simulations for $p(\Omega)$ as a function of both driving frequency ω and response frequency Ω over a range of parameters analogous to those shown in Fig. 1. We discuss these transitions one by one (see also section I.C of the Supplemental Material). When driving at ω leads to a response in the dipole $p(t)$ at a frequency Ω such that $\omega = \Omega = E_Z$, a pure spin transition is induced. This corresponds to the fundamental resonances (1,2). The first subharmonic response occurs when $\omega = \Omega/2 = E_Z/2$, which is the case of resonances (3,4). For the second subharmonic, resonances (9,10), we have $\omega = \Omega/3 = E_Z/3$. All the transitions discussed so far are adiabatic in the orbital sector. However, transitions that are non-adiabatic in the orbital sector are also allowed, i.e. transitions where an orbital excitation is involved (in the experiment, this would correspond to a valley excitation, the valley being the lowest energy orbital-like excitation). First, $\Omega = E_{01}$, a pure orbital excitation is induced (a pure valley transition with excitation energy E_{VS} in the experiment), which is magnetic field independent and occurs over a wide range of ω. This is transition (7) in Figs. 2(c). Next, resonance (5) runs parallel to the fundamental resonance, with $\omega = \Omega - E_{01}$ and furthermore $\Omega = E_Z$, so that $\omega = E_Z - E_{01}$. Thus driving at frequency ω induces a spin excitation and an

orbital (valley) de-excitation, see the double red arrow in Fig. 1(d). We call this process inter-valley spin resonance. Finally, resonance (6), which runs parallel to (9,10), is characterised by $\omega = \Omega/3 + E_{01}/3$, again with $\Omega = E_Z$. Here, driving at ω leads to a spin excitation and an orbital excitation. The upper inset of Fig. 2(b) highlights the particular resonances in the main figure that should be compared to the experimental data shown in Fig. 1(a,b).

An interesting feature of the resonances, observed both in the experiments and theory (Figs. 2(b-d)), is the apparent 'level repulsion' between resonance lines (5) and (6) that takes place near $B_{tot} = 480$ mT. This magnetic field value is much higher than $E_{VS}/g\mu_B \sim B_{tot} = 250$ mT, where the anti-crossing between the states $|v_1,\downarrow\rangle$ and $|v_2,\uparrow\rangle$ is expected to occur [15] (see the red dashed line in Fig. 1(d)), but which is outside our measurement window, see above. Instead the observed 'level repulsion' has a purely dynamical origin, as demonstrated by the fact that the anti-crossing is suppressed in Fig. 2(c), where the simulation parameters are identical to Fig. 2(b), except for a smaller driving amplitude ϵ_1.

In Sec. II of the Supplemental Material, we develop a dressed-state theory to describe these strong-driving effects. In this formalism, the quasiclassical driving field of Eq. 2 is replaced by a fully quantum description of the photon field and its coupling to the (valley)-orbital Hamiltonian of the quantum dot. The resulting dressed eigenstates describe the hybridized photon-orbital levels, and more generally, the hybridization of orbital, photon, and spin states. In this way, resonances (1) and (2) in Fig. 2(c) correspond to single-photon spin flips, while resonances (3) and (4) correspond to two-photon spin flips. Resonance (5) involves both a spin flip and a valley-orbit excitation and is parallel to resonance (1,2), indicating that it is a single-photon process. Resonance (6) is parallel to (9,10), indicating that it is a three-photon process. The physical mechanisms of the resonances are also indicated in Fig. 1(d).

In principle, coupling occurs between all of the dressed states due to the effective spin-orbit coupling in our EDSR experiment. In practice however, the orbital-Rabi frequency is two orders of magnitude larger than the spin-Rabi frequency, so mode hybridization is only observed between resonance (5) and (6), resulting in the level repulsion. The magnitude of this repulsion provides a convenient way to determine the orbital-Rabi frequency, which cannot be measured directly due to the fast dephasing of the excited valley-orbit state (see section III). In Sec. II of the Supplemental Material, we estimate this Rabi frequency to be about 0.2 GHz.

COHERENCE OF THE INTER-VALLEY SPIN TRANSITION

We now examine the possible origin of the ten times larger line width of resonance (5) compared to that of the pure spin-flip resonances (1) and (2). Given the partial valley nature of transition (5) and the strong valley-orbit coupling that is typical of Si/SiGe quantum dots [15, 16, 36], a plausible candidate decoherence mechanism for this transition is electric field noise.

In order to study the sensitivity to electric fields of the respective transitions, we show in Fig. 3(a) the dependence of the frequency of resonances (1) and (5) on the voltage applied to one of the quantum dot gates, V_2. Clearly, resonance (5) exhibits a much greater sensitivity to gate voltage than resonance (1): ~ 18.5 MHz/mV for $f_0^{(5)}$, versus ~ 0.5 MHz/mV for $f_0^{(1)}$. We also notice that the two resonance shifts as a function of V_2 have opposite sign, which indicates that different mechanisms are responsible. For resonance (1), we believe that the dominant effect of the electric field is the displacement of the electron wave function in the magnetic field gradient from the micromagnets [17] (see section III.B of the Supplemental Material). This effect also contributes to the frequency shift of resonance (5), but presumably it is masked by the change in valley-orbit splitting (E_{VS}) resulting from the displacement of the electron wave function in the presence of interface disorder [11, 37]. For instance, moving the electron towards or away from a simple atomic step at the Si/SiGe interface leads to a change of the valley-orbit energy splitting, as shown by the results of numerical simulations reported in Fig. 3(b,c) [38]. As expected, the simulations predict a minimum in the valley-orbit splitting when the wave function is centered around the atomic step, but interestingly it does not vanish, i.e. the opposite signs for the valley-orbit splitting left and right of the atomic step do not lead to complete cancellation (see section IV of the Supplemental Material for a more detailed description).

The $\sim$35 times greater sensitivity of the spin-valley transition frequency to electric fields may contribute to its ten times larger line width compared to the intra-valley spin transition. The line width of the intra-valley spin transition is believed to be dominated by the 4.7% ^{29}Si nuclear spins in the host material [17]. The nuclear field also affects the spin-valley transition, but obviously only accounts for a small part of the line width here. We propose that the dominant contribution to the line width of resonance (5) is low-frequency charge noise.

Although not definitive, some evidence for this interpretation is found in Fig. 3(d), which shows a scatter plot of $f_0^{(5)}$ and one of the dot-reservoir tunnel rates, simultaneously recorded over many hours (see section III.C of Supplemental Material for a more detailed description of the measurement scheme). The dot-reservoir tunnel rate

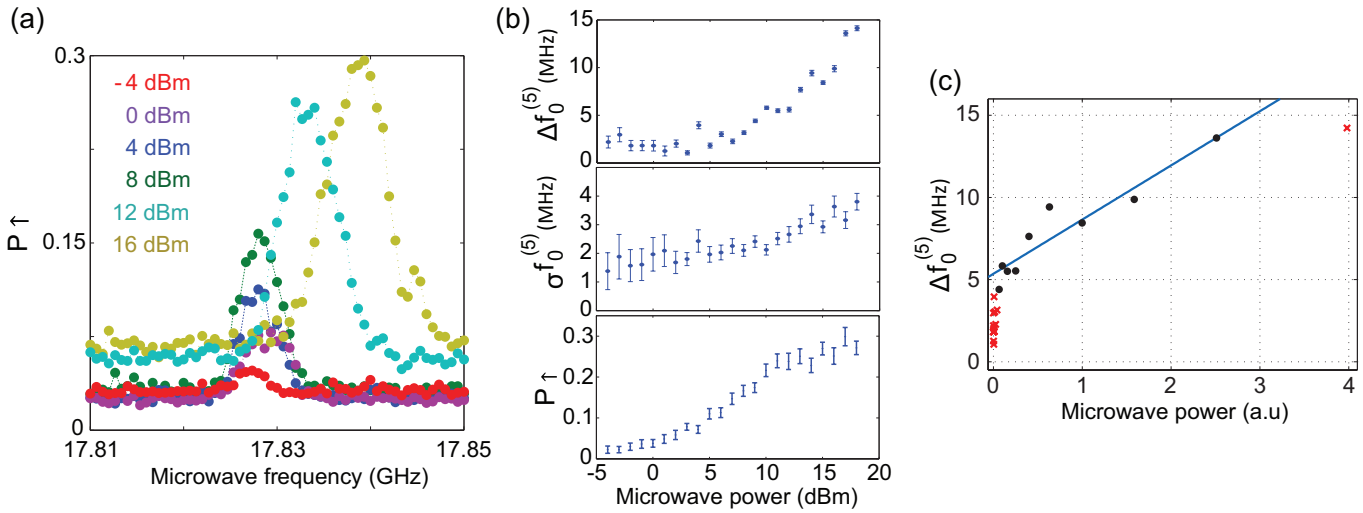

FIG. 4. (a) Measured spin-up probability as a function of microwave power at $B_{ext}^{y} = 846$ mT for a fixed microwave burst time of 50 μs, near the resonance condition for inter-valley spin-flip transition (5). For increasing power, the line does not only become taller and wider but also moves towards higher frequencies. Panel (b) summarizes from top to bottom the center frequency, width and height of the response. $\Delta f_0^{(5)} = f_0^{(5)} - 17.825$ GHz. (c) Top panel of figure (b) replotted using a linear power scale (x-axis $\propto 10^{\mathbf{MW\ power(dBm)}/5}$). The blue line represents a linear fit to the black data points to the relation $\Delta E_{\text{asymp}} \propto \epsilon_1^2$ (eq. S42). The points indicated by the red crosses are excluded from the fit.

serves as a sensitive probe of local electric fields, including those produced by charges that randomly hop around in the vicinity of the quantum dot (see Fig. S6) [39]. The plot shows a modest correlation between the measured tunnel rate and $f_0^{(5)}$, suggesting that the shifts in time of both quantities may have a common origin, presumably low-frequency charge noise.

In this case, we can also place an upper bound on T_2^* permitted by charge noise for the intra-valley spin transitions (1,2) in the present sample (given the specific magnetic field gradient reported in [17]). Indeed, due to the micro magnet induced gradient in the local magnetic field parallel to B_{ext}, the pure spin transitions are also sensitive to charge noise. Given that $T_2^* \sim 110$ ns for transition (5) and the ratio of ~ 35 in sensitivity to electric fields, charge noise in combination with this magnetic field gradient would limit T_2^* to ~ 3.8 μs for transitions (1,2). It is important to note that this is not an intrinsic limitation, as the stray field of the micro magnet at the dot location can be engineered to have zero gradient of the longitudinal component, so that to first order charge noise does not affect the frequency and T_2^* of transitions (1,2). At the same time, a strong gradient of the transverse component can be maintained, as is necessary for driving spin transitions.

Besides its strong sensitivity to static electric fields, we report a surprising dependence of the frequency of resonance (5) on microwave driving power [Fig. 4(b,c)]. Increasing the driving power, the resonance not only broadens but also shifts in frequency, as in an a.c. Stark shift [40]. This dynamical evolution is very different from the case of the intra-valley spin resonance, which is power broadened but stays at fixed frequency [8, 17]. This frequency shift is, at least for a limited microwave power range, in line with the dynamical level repulsion captured by Eq. S42, where $\Delta E_{\text{asymp}} \propto \epsilon_1^2$ expresses the energy splitting between resonance (5) and its asymptote, $\hbar\omega = E_Z - E_{01}$. This relation is verified in Fig. 4(c) for microwave powers of $9 - 17$ dBm.

Finally, we attempt to drive coherent oscillations using resonance (5) at high applied microwave power, recording the spin excited state probability as a function of the microwave burst time. Oscillations are not visible, indicating that the highest Rabi frequency we can obtain for resonance (5) is well below the corresponding $1/T_2^*$ of 110 ns. This is consistent with our estimate that the Rabi frequency is of the order of 10 kHz, based on the magnitude of the dynamical level repulsion seen in Fig. 1(a,b) and the derivation in the section II.B of Supplemental Material.

CONCLUSIONS

Despite its simplicity, the electrical driving of a single electron confined in a single quantum dot can produce a complex spin resonance energy spectrum. This particularly applies for quantum dots realized in silicon, where the presence of the excited valley-orbit state, close in energy and strongly coupled to the ground state, introduces a substantial non-linearity in the system response to microwave electric fields. This allows us to observe

a transition whereby both the spin and the valley state are flipped at the same time. We demonstrate how both static external electric fields and electrical noise influence the frequency of this inter-valley spin transition, limiting its coherence properties and its potential utility as a qubit [25].

Much of the dynamics of the spin and valley transitions can be captured in a semi-classical picture, including driving using higher harmonics exploiting non-linearities. However, under intermediate or strong driving, new phenomena emerge that cannot be easily explained except in terms of dressed states that fundamentally involve a quantum mechanical coupling between photons and orbital or spin states. Here, we have provided experimental and numerical evidence for the existence of such dressed states of photons and valley-orbit states at strong driving. We have further estimated the strength of this valley-orbit to photon coupling by comparing our analytical theory to the experiments.

This work provides important experimental and theoretical insight in the role of inter-valley transitions for controlling spin dynamics in silicon based quantum dots. It also highlights the limitations of valley-based qubits in the presence of strong valley-orbit coupling, due to their sensitivity to electrical noise.

ACKNOWLEDGMENTS

We acknowledge R. Schouten and M. J. Tiggelman for technical support and the members of the Delft spin qubit team for useful discussions. Research was supported by the Army Research Office (W911NF-12-0607), a European Research Council Synergy grant, and the Dutch Foundation for Fundamental Research on Matter. E.K. was supported by a fellowship from the Nakajima Foundation. The development and maintenance of the growth facilities used for fabricating samples is supported by DOE (DE-FG02-03ER46028), and this research utilized NSF-supported shared facilities at the University of Wisconsin-Madison.

[1] K. C. Nowack, F. H. L. Koppens, Y. V. Nazarov, and L. M. K. Vandersypen, "Coherent control of a single electron spin with electric fields." Science **318**, 1430 (2007).

[2] E. A. Laird, C. Barthel, E. I. Rashba, C. M. Marcus, M. P. Hanson, and A. C. Gossard, "A new mechanism of electric dipole spin resonance: hyperfine coupling in quantum dots," Semiconductor Science and Technology **24**, 064004 (2009).

[3] F. Pei, E. A. Laird, G. A. Steele, and L. P. Kouwenhoven, "Valleyspin blockade and spin resonance in carbon nanotubes," Nat. Nanotechnol. **7**, 630–634 (2012).

[4] E. A. Laird, F. Pei, and L. P. Kouwenhoven, "A valleyspin qubit in a carbon nanotube," Nat Nanotechnol. **8**, 565–568 (2013).

[5] J. Stehlik, M. D. Schroer, M. Z. Maialle, M. H. Degani, and J. R. Petta, "Extreme Harmonic Generation in Electrically Driven Spin Resonance," Phys. Rev. Lett. **112**, 227601 (2014).

[6] S. Nadj-Perge, V. S. Pribiag, J. W. G. van den Berg, K. Zuo, S. R. Plissard, E. P. A. M. Bakkers, S. M. Frolov, and L. P. Kouwenhoven, "Spectroscopy of Spin-Orbit Quantum Bits in Indium Antimonide Nanowires," Phys. Rev. Lett. **108**, 166801 (2012).

[7] F. Forster, M. Mühlbacher, D. Schuh, W. Wegscheider, and S. Ludwig, "Electric-dipole-induced spin resonance in a lateral double quantum dot incorporating two single-domain nanomagnets," Phys. Rev. B **91**, 195417 (2015).

[8] P. Scarlino, E. Kawakami, D. R. Ward, D. E. Savage, M. G. Lagally, Mark Friesen, S. N. Coppersmith, M. A. Eriksson, and L. M. K. Vandersypen, "Second-Harmonic Coherent Driving of a Spin Qubit in a Si/SiGe Quantum Dot," Phys. Rev. Lett. **115**, 106802 (2015).

[9] A. V. Khaetskii and Y. V. Nazarov, "Spin-flip transitions between Zeeman sublevels in semiconductor quantum dots," Phys. Rev. B **64**, 125316 (2001).

[10] Mark Friesen, M. A. Eriksson, and S. N. Coppersmith, "Magnetic field dependence of valley splitting in realistic SiSiGe quantum wells," Appl. Phys. Lett. **89**, 202106 (2006).

[11] Mark Friesen and S. N. Coppersmith, "Theory of valley-orbit coupling in a Si/SiGe quantum dot," Phys. Rev. B **81**, 1–17 (2010).

[12] S. Goswami, K. A. Slinker, Mark Friesen, L. M. McGuire, J. L. Truitt, C. Tahan, L. J. Klein, J. O. Chu, P. M. Mooney, D. W. van der Weide, R. Joynt, S. N. Coppersmith, and Mark A. Eriksson, "Controllable valley splitting in silicon quantum devices," Nat. Phys. **3**, 41–45 (2007).

[13] F. A. Zwanenburg, A. S. Dzurak, A. Morello, M. Y. Simmons, L. C. L. Hollenberg, G. Klimeck, S. Rogge, S. N. Coppersmith, and M. A. Eriksson, "Silicon quantum electronics," Reviews of Modern Physics **85**, 961–1019 (2013).

[14] M. J. Rančić and G. Burkard, "Electric dipole spin resonance in systems with a valley-dependent g factor," Phys. Rev. B **93**, 205433 (2016).

[15] C. H. Yang, A. Rossi, R. Ruskov, N. S. Lai, F. A. Mohiyaddin, S. Lee, C. Tahan, G. Klimeck, A. Morello, and A. S. Dzurak, "Spin-valley lifetimes in a silicon quantum dot with tunable valley splitting," Nat. Commun. **4** (2013).

[16] X. Hao, R. Ruskov, M. Xiao, C. Tahan, and H. Jiang, "Electron spin resonance and spinvalley physics in a silicon double quantum dot," Nat. Commun. **5** (2014).

[17] E. Kawakami, P. Scarlino, D. R. Ward, F. R. Braakman, D. E. Savage, M. G. Lagally, Mark Friesen, S. N. Coppersmith, M. A. Eriksson, and L. M. K. Vandersypen, "Electrical control of a long-lived spin qubit in a Si/SiGe quantum dot," Nat. Nanotechnol. **9**, 666–670 (2014).

[18] M. Veldhorst, J. C. C. Hwang, C. H. Yang, A. W. Leenstra, B. de Ronde, J. P. Dehollain, J. T. Muhonen, F. E. Hudson, K. M. Itoh, A. Morello, and A. S. Dzurak, "An addressable quantum dot qubit with fault-tolerant control-fidelity," Nat. Nanotechnol. **9**, 981–985 (2014).

[19] M. Veldhorst, R. Ruskov, C. H. Yang, J. C. C. Hwang, F. E. Hudson, M. E. Flatté, C. Tahan, K. M. Itoh, A. Morello, and A. S. Dzurak, "Spin-orbit coupling and operation of multivalley spin qubits," Phys. Rev. B **92**, 201401 (2015).

[20] R. J. Warburton, "Single spins in self-assembled quantum dots," Nat. Mater. **12**, 483–493 (2013).

[21] T. Fujisawa, D. G. Austing, Y. Tokura, Y. Hirayama, and S. Tarucha, "Allowed and forbidden transitions in artificial hydrogen and helium atoms," Nature **419**, 278–281 (2002).

[22] A. C. Johnson, J. R. Petta, J. M. Taylor, A. Yacoby, M. D. Lukin, C. M. Marcus, M. P. Hanson, and A. C. Gossard, "Triplet-singlet spin relaxation via nuclei in a double quantum dot," Nature **435**, 925–928 (2005).

[23] L. R. Schreiber, F. R. Braakman, T. Meunier, V. Calado, J. Danon, J. M. Taylor, W. Wegscheider, and L. M. K. Vandersypen, "Coupling artificial molecular spin states by photon-assisted tunnelling," Nat. Commun. **2**, 556 (2011).

[24] F. R. Braakman, J. Danon, L. R. Schreiber, W. Wegscheider, and L. M. K. Vandersypen, "Dynamics of spin-flip photon-assisted tunneling," Phys. Rev. B **89**, 075417 (2014).

[25] D. Culcer, A. L. Saraiva, B. Koiller, X. Hu, and S. Das Sarma, "Valley-Based Noise-Resistant Quantum Computation Using Si Quantum Dots," Phys. Rev. Lett. **108**, 126804 (2012).

[26] Y. Tokura, W. G. van der Wiel, T. Obata, and S. Tarucha, "Coherent Single Electron Spin Control in a Slanting Zeeman Field," Phys. Rev. Lett. **96**, 047202 (2006).

[27] M. Pioro-Ladrière, T. Obata, Y. Tokura, Y. S. Shin, T. Kubo, K. Yoshida, T. Taniyama, and S. Tarucha, "Electrically driven single-electron spin resonance in a slanting Zeeman field," Nat. Phys. **4**, 776–779 (2008).

[28] Here, we present measurements realized for different magnetic field orientations. The components of the external magnetic field are reported in each figure. The specific orientation of the external magnetic field does not play any special role. It is our understanding that the results presented in this work are independent from the specific magnetic field orientation.

[29] E. I. Rashba, "Mechanism of half-frequency electric dipole spin resonance in double quantum dots: Effect of nonlinear charge dynamics inside the singlet manifold," Phys. Rev. B **84**, 241305 (2011).

[30] For resonance (5), the valley state must flip too; therefore, a spin-valley coupling mechanism is required [15, 16, 41].

[31] For a charge qubit, L is the lateral separation between the two sides of the double quantum dot. For an orbital qubit, L is the lateral separation of the center of mass of the two orbital states. For a pure valley qubit, L is the vertical separation of the even and odd states ($\sim$0.16 nm). For a complicated system like a valley-orbit qubit with interface disorder, L will have lateral and vertical components, with the lateral component being usually much larger than the vertical one. In this last case the exact length L will depend on the specifics of the interface disorder; a reasonable guess would be $L \sim$0.5-5 nm (see, e.g. Ref. [36]).

[32] L. Landau, Phys. Z. Sowjetunion **32**, 46 (1932).

[33] C. Zener, "Non-Adiabatic Crossing of Energy Levels," Proceedings of the Royal Society A: Mathematical, Physical and Engineering Sciences **137**, 696–702 (1932).

[34] E. C. G. Stuckelberg, Helv. Phys. Acta **5**, 369 (1932).

[35] For the Hamiltonian parameters indicated in the caption of Fig. 2(b), we use time steps in the range 0.061-0.073.

[36] J. K. Gamble, M. A. Eriksson, S. N. Coppersmith, and Mark Friesen, "Disorder-induced valley-orbit hybrid states in Si quantum dots," Phys. Rev. B **88**, 035310 (2013).

[37] Z. Shi, C. B. Simmons, J. R. Prance, J. K. Gamble, T. S. Koh, Y. P. Shim, Xuedong Hu, D. E. Savage, M. G. Lagally, M. A. Eriksson, Mark Friesen, and S. N. Coppersmith, "Fast Hybrid Silicon Double-Quantum-Dot Qubit," Phys. Rev. Lett. **108**, 140503 (2012).

[38] P. Boross, G. Széchenyi, D. Culcer, and A. Pályi, "Control of valley dynamics in silicon quantum dots in the presence of an interface step," Phys. Rev. B **94**, 035438 (2016).

[39] L. M. K. Vandersypen, J. M. Elzerman, R. N. Schouten, L. H. Willems van Beveren, R. Hanson, and L. P. Kouwenhoven, "Real-time detection of single-electron tunneling using a quantum point contact," Appl. Phys. Lett. **85**, 4394 (2004).

[40] M. Brune, P. Nussenzveig, F. Schmidt-Kaler, F. Bernardot, A. Maali, J. M. Raimond, and S. Haroche, "From Lamb shift to light shifts: Vacuum and subphoton cavity fields measured by atomic phase sensitive detection," Phys. Rev. Lett. **72**, 3339–3342 (1994).

[41] P. Huang and X. Hu, "Spin relaxation in a Si quantum dot due to spin-valley mixing," Phys. Rev. B **90**, 235315 (2014).